Opportunities and Challenges of Spaceborne Sensors in Delineating Land Surface Temperature Trends: A Review

M. Razu Ahmed, Ebrahim Ghaderpour, Anil Gupta, Ashraf Dewan, and Quazi K. Hassan

***Abstract*—Understanding the land surface temperature (LST) trends is crucial for policymakers and stakeholders to develop adaptation and mitigation strategies suitable for a sustainable environment coping in the face of climate change. This article presents a systematic review of the studies related to delineating spaceborne sensor-based LST trends, including information on the instruments and constellations of satellites (missions) that provide thermal infrared (TIR) and passive microwave (PMW) observations. About 99% of the studies used TIR, where 76% were Moderate Resolution Imaging Spectroradiometer (MODIS, onboard Terra/Aqua) observations. Opportunities, challenges, and research gaps for using the TIR and PMW observations were also explored, with instruments onboard either polar-orbiting or geostationary satellites. We identified that the calibrated dataset (e.g., processed, harmonized, and standardized) is extremely limited for each constellation, with multiple satellites and instruments, to make it fully useful for the entire mission period. A few problematic methodological concepts were identified, including using a few images in a longer time series. Using only a few images, acquired on different calendar months in different years, would not provide the true annual trends over the study period because they can be influenced by seasonal variations. To estimate the warming or cooling daytime, nighttime, or diurnal LST trends, the use of MODIS observations could be useful, even though it does not acquire images during the maximum or minimum temperature in a daily cycle. This article indicated further investigations into those research gaps and recommended directions to overcome most of these limitations.**

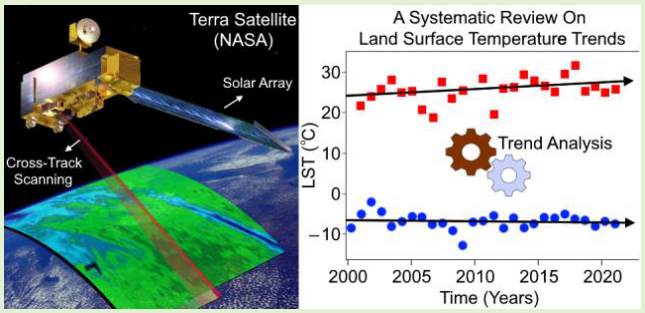

***Index Terms*—Land surface temperature (LST), Moderate Resolution Imaging Spectroradiometer (MODIS), passive microwave (PMW), thermal infrared (TIR), trend.**

I. Introduction

TEMPERATURE trends, the spatiotemporal variations of temperature over a longer period, are the key indicator of representing climate change [1]. While land surface temperature (LST) is dependent on the spatial variability of solar radiation and land–atmosphere heat exchange [2], the temporal variability of solar might has effects on the Earth's climate [3]. Spatiotemporal distributions of LST reflect not only the variations of climatic factors but also the characteristics of land surface [4].

It has interdependence among climate, ecosystems, biodiversity, and human societies. It can directly or indirectly impact many aspects of society by potentially disrupting the normal natural balance and forcing the change of weather patterns [5]. Increasing temperature trends (warming) and other associated factors are threatening human existence, ecological communities, and socioeconomic development across the world [6]. The Intergovernmental Panel on Climate Change (IPCC) reported that the global mean temperature had risen (global warming) by about 0.85 (±0.2) °C from 1880 to 2012 [1], [7]. Knowing the magnitude and rate of temperature change (temperature trend) would guide the formulation of appropriate levels of mitigation and adaptation strategies.

Manuscript received 21 January 2023; accepted 16 February 2023. Date of publication 24 February 2023; date of current version 31 March 2023. This study was partially funded by a Discovery Grant from the Natural Sciences and Engineering Research Council of Canada to Q.K. Hassan. The associate editor coordinating the review of this article and approving it for publication was Prof. Huang Chen Lee. *(Corresponding author: Quazi K. Hassan.)*

M. Razu Ahmed and Quazi K. Hassan are with the Department of Geomatics Engineering, Schulich School of Engineering, University of Calgary, Calgary, AB T2N 1N4, Canada (e-mail: mohammad.ahmed2@ucalgary.ca; qhassan@ucalgary.ca).

Ebrahim Ghaderpour is with the Department of Earth Sciences, Sapienza University of Rome, 00185 Rome, Italy (e-mail: ebrahim.ghaderpour@uniroma1.it).

Anil Gupta is with the Resource Stewardship Division, Alberta Environment and Protection Areas, Calgary, AB T2L 2K8, Canada (e-mail: anil.gupta@gov.ab.ca).

Ashraf Dewan is with the Spatial Sciences Discipline, School of Earth and Planetary Sciences, Curtin University, Bentley, WA 6102, Australia (e-mail: a.dewan@curtin.edu.au).

Digital Object Identifier 10.1109/JSEN.2023.3246842

It would help minimize the rate magnitude of the changes to keep our globe a habitable place through a sustainable environment [5].

In determining the temperature trends, the method of using in situ measurements of weather stations is the most accurate approach for the station locations. To represent trends, studies used interpolation techniques to derive the temperature for the remaining landscape [8]. The use of interpolation values in determining the temperature trends has some issues, e.g., various interpolation techniques, such as polynomial, nearest neighbor, and Fourier methods, produce different outputs even using the same input data [9], [10]. Considering this, another efficacious alternative is to use spaceborne sensor-derived LST for estimating temperature trends at regular grids, covering nearly the entire globe. A review article [11] also indicated the importance of using spaceborne Earth observational sensors by quantifying the performances and limitations of different methods used in the literature for LST trend analysis. In general, studies in the literature used the Mann–Kendall (MK) test, Sen's slope estimator (SSE), and linear regression methods to determine the trends of LST [12]. The MK test and SSE have the advantage that they can be applied independent of data distribution pattern in the time series, in contrast to the linear regression analysis whose statistical testing depends on the normality assumption [12]. Because of the nonparametric characteristic of the LST data, the MK test was mostly used to detect the trends in time series, including the SSE to determine the upward or downward directions of trend, i.e., positive or negative slope, respectively. However, the MK test may fail for time series with seasonality and may give incorrect results for shorter time series due to serial correlations [13], see also Section VII showing a simulation experiment.

Spaceborne remote sensors operating in specific wavelength ranges, including thermal infrared (TIR, 8–14 μm) and passive microwave (PMW, 0.8–75 cm or frequency 0.4–35 GHz), are useful in studying LST trends at a pleasant spatial resolution. The polar-orbiting satellites can observe both TIR and PMW, and geostationary satellites only TIR. While the datasets derived from these platforms have created opportunities for delineating the LST trends, challenges exist due to lack of long time series from a single instrument, differences in both spatial and temporal resolutions among the datasets. Here, the aim was to understand the opportunities and challenges of using remote sensing-derived LST data in delineating its trends. Hence, the specific goals were to: 1) conduct a systematic review on the LST trends reported in the literature using both TIR and PMW instruments; 2) opportunities and challenges of using the LST time series data; and 3) determine research gaps in the appropriate use of remote sensing data and summarize future research potentials.

II. Systematic Review

Web of Science (WoS) and Scopus are the two widely used citation and publication databases. Here, we used the Scopus database for the search of relevant publications, due to its broader coverage of publications with 20% more than WoS [14]. In Scopus, we performed the following search in Title-Abstract-Keyword on June 24, 2022: (LST)

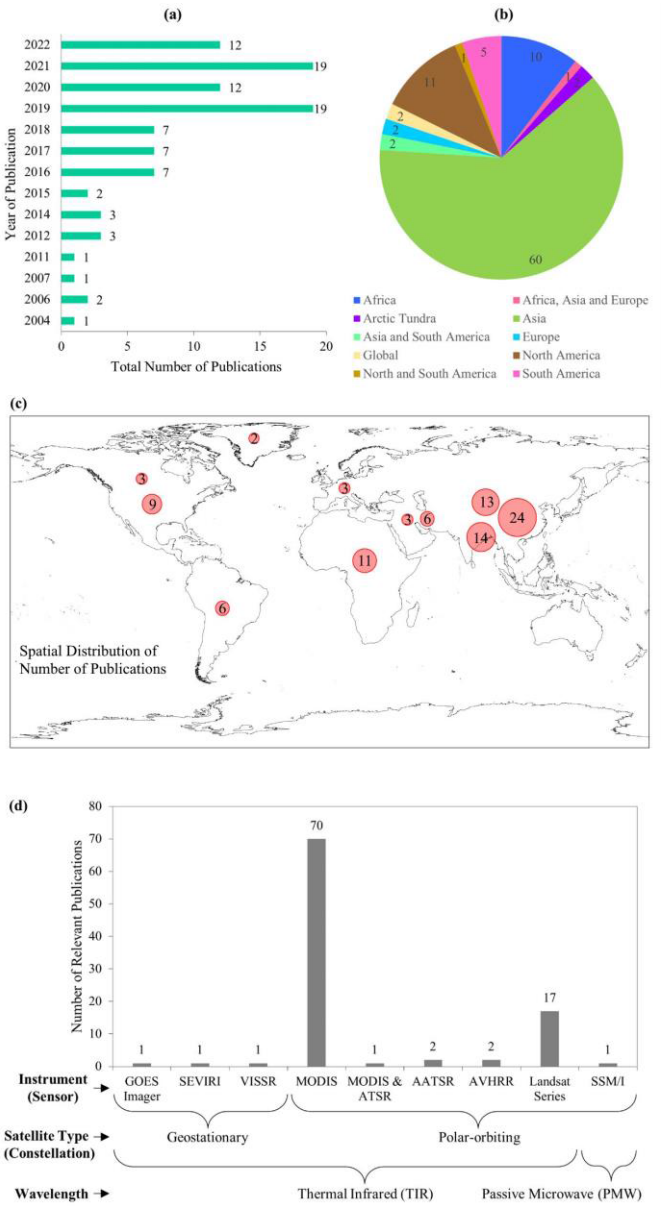

Fig. 1. (a) Annual count of articles. (b) Location of the study area on the continents or greater regional scale. (c) Spatial distribution of publications. (d) Sensor-wise count of articles.

and ("warming trend*" or "cooling trend*" or "temperature trend*" or "positive trend*" or "negative trend*") and not ("ocean" or "lake"). This search returned 174 documents, including 148 English articles, 12 conference papers, three book chapters, two review articles, one letter, and eight non-English articles, where the English articles were analyzed further. Among these, 31 articles did not use remote sensing data, and another 21 articles used remote sensing data but did not perform trend analysis. Therefore, we considered a total of 96 relevant articles in this study. Note that other keywords, such as spatiotemporal and cloud computing, were also searched along with LST and trend, but all results were captured by the keywords mentioned earlier. The first article was published in 2004, and the total number of articles published per year was the highest in the last four years (2019–2022) [see Fig. 1(a)]. National Oceanic and Atmospheric Administration (NOAA) polar-orbiting environmental

satellites have been providing LST data since the 1980s, and thus, a steady increasing trend of using them was observed in the literature. The trend of publishing the related articles, started in 2004, may be linked to the cost-free data availability to scientists around the first decade of this century. It is likely that the LST trend related works will be published more in the coming years. Nevertheless, in terms of the location of study area, the most publications were in Asia (60), followed by North America (12) and Africa (11) [see Fig. 1(b)]. In Asia, studies were mostly conducted in China (24), the Tibetan Plateau (13), South India (14), and Iran (6), and middle eastern countries (3) [see Fig. 1(c)]. Also, the sensor-wise group of articles for TIR and PMW instruments onboard polar-orbiting and geostationary satellites is shown in Fig. 1(c), which is discussed in Sections III and IV.

III. TIR-Based Studies

Fig. 1(d) shows that 95 out of 96 articles used TIR instruments in studying the LST trends, where 92 articles were derived from polar-orbiting satellites [see Fig. 1(c)]. Among the polar-orbiting satellites, the sensors included: 1) Moderate Resolution Imaging Spectroradiometer (MODIS); 2) Landsat instrument series—Thematic Mapper (TM), Enhanced TM Plus (ETM+), TIR Sensor (TIRS), and TIRS2; 3) Along Track Scanning Radiometers (ATSRs) and Advanced ATSR (AATSR); and 4) Advanced Very High Resolution Radiometer (AVHRR) instruments.

A. Moderate Resolution Imaging Spectroradiometer

MODIS-derived LST is the most common in the literature (i.e., 71 articles) to delineate LST trends since 2000. Most of the studies were conducted in China (∼27%), Tibetan Plateau (∼13%), and India (∼11%), while two studies were on the global scale [15], [16]. A good number of studies focused on LST trends in the landscapes [17], [18], [19], [20], [21], [22], [23], [24], [25], [26], [27], [28], [29], [30], [31], [32], along with other trends, such as evapotranspiration [33], [34] and rainfall and vegetation [35], and water balance components, such as precipitation, snow cover, and stream flows [34]. Studies of MODIS LST trends in urban areas or cities, especially larger in size, were also found [36], [37], [38], [39]. In the urban/city, studies focused on urban heat island (UHI) [40], [41], [42], [43], surface UHI (SUHI) [44], [45], [46], [47], [48], [49], [50], and urban expansion [51]. Studies showed the impacts on LST trends due to the physical changes in wetland [52], [53], [54], land cover [1], [5], [55], forest cover [56], elevation [29], [57], [58], [59], and hydroelectric projects [60]. Two very recent publications also investigated the LST trends over India and South Asia [1], [5]. Vegetation has demonstrated a significant role in influencing the cooling or warming trends in many parts of the world [61], [62], [63], [64], [65], [66], [67], [68], [69]. Some studies have linked LST trends with changes in soil moisture [70], drought conditions [71], and desertification [72]. Studies have also been conducted finding relationships of temperature trends with wind firms [73], [74], [75], earthquake impact [76], CO_2 emission [77], and vector-borne diseases [78]. Driving factors or causes of warming or cooling trends were also studied [19], [33], [46], [49], [79], [80], [81]. Most of these studies were conducted using MODIS LST data with a spatial resolution of 1 km and a few with 5.6 km. To further improve the spatial resolution of the temperature trends, a study performed a downscaling (from 1 km to 240 m) approach using the adaptive random forest regression method [82]. Some of the studies are summarized in Table I.

B. Landsat

Landsat was the second most (∼18%) instrument to delineate LST trends [see Fig. 1(c)]. Because of the finer spatial resolutions (30–120 m) compared to MODIS, Landsat-derived LST was mostly used in urban-related studies using at least two images. To study the urban impact on LST, 16 images were used in obo-Dioulasso (Burkina Faso, Sub-Shaharan Africa) over 22 years (1991–2013) [83], 11 images in the semiarid city Erbil, Iraq over 21 years (1992–2013) [84], and two images in Changchun, China, over 12 years (1993–2005) [85]. Also, an LST trend analysis was performed in urban areas (cities) in Ghana [86], India [87], Iran [88], Thailand [89], and USA [90], [91] using variable numbers of Landsat images in the study periods, i.e., three in six, eight (two in each year) in 30, four in 30, six in 10, and 53 in five years, respectively. Other studies performed LST trends in finding relationships with land use land cover changes (LULCs) [92], [93], forest cover changes [94], and changes in normalized difference vegetation index (NDVI) [95], [96], [97] and green roof [98]. Using 364 images (aggregated for each of the months) of Landsat time series over the 2000–2010 period, Reyes et al. [99] showed that urban irrigation suppressed the LST regimes. Some of the studies using Landsat are summarized in Table II.

C. Along Track Scanning Radiometer

Three studies, i.e., one ATSR (onboard European Remote-Sensing Satellite—ERS) and two AATSR (onboard ENVISAT—Environmental satellite), used LST time series from the European Space Agency (ESA) mission [see Fig. 1(c)]. The ATSR (along with MODIS) LST time series over 2003–2011 at 1 km was used to determine the monthly minimum and maximum trends in China [100]. LST time series datasets of the AATSR instrument at 1 km were utilized for trends—across elevation changes in the Tibetan Plateau during 2003–2011 [101] and the Heihe River Basin, China, during 2002–2012 [102].

D. Advanced Very High Resolution Radiometer

We found two studies that used AVHRR data from the NOAA mission [see Fig. 1(c)]. Bhatt et al. [103] used AVHRR-derived LST at 1.1 km from NOAA-7 through NOAA-18 satellites over the 1982–2015 period to study Arctic tundra vegetation productivity. They showed a positive trend for 1982–1998 during growing seasons, and 1999–2015 were positive in May–June but slightly negative for July–August. In another study, Pinheiro et al. [104] delineated warming and cooling trends over Continental Africa during the 1995–2000 period using a 4-km LST product of daily day and nighttime NOAA-14 AVHRR/2 instrument.

TABLE I
SELECTED PUBLICATIONS ALONG WITH THEIR KEY FINDINGS FOR MODIS-BASED LST TREND ANALYSIS

Ref.	Location & Period	Product & Resolution	Method	Key findings
[44]	Mediterranean cities (2001-2012)	MOD11A2-V5 8-day at 1 km	Linear regression	LST is utilized to investigate surface urban heat island in 17 major Mediterranean cities. Increasing LST trends were observed in most of the cities which were correlated with urban development indicators.
[82]	Iran (2001-2019)	MOD11A1-V6 Daily at 1 km		Positive and negative LST trends were estimated across Iran during a full year, spring, summer, fall, and winter. An adaptive random forest regression method was developed for LST downscaling at national scale.
[62]	Continental USA (2003-2016)	MOD11A2-V6 8-day at 1 km		Warming and cooling influenced vegetation growth over the continental US. About 58% of the continental US showed a positive LST trend more significantly in the western US. About 35% portion had a negative LST trend, particularly in the Northern Rockies and Plains and in the Upper Midwest.
[30]	Middle East Countries (2001-2018)	MOD11A2-V6 8-day at 1 km		Winters in the middle east countries, such as Iran, Israel, and Jordan have become milder. Negative trends were observed in the spring LST in Bahrain and Oman and the summer LST in Bahrain and Qatar. Iraq showed a positive LST trend.
[27]	China (2003-2019)	MOD11A2-V6 8-day at 1 km		Daytime and nighttime LST trend was reverse in Fall. LST showed an increasing trend in all seasons except the daytime in Fall. Years 2017 and 2011 exhibited the turning LST trends. Vegetation and air temperature were the main factors impacting LST.
[58]	Andean region in S. America (2000-2017)	MOD11A2-V6 8-day at 1 km	Mann-Kendall and Sen's slope trend analysis	Winter daytime LST depended on elevation with strongest warming at higher elevations. Winter nighttime LST trend was slightly increasing by altitude
[46]	Bangladesh (2000-2019)	MOD11A2-V6 8-day at 1 km		Positive daytime LST trend was reported for four major cities in Bangladesh, and one city showed a negative nighttime LST trend. Population, lack of vegetation, and anthropogenic activities were the main drivers of urban warming.
[12]	Canada (2001-2020)	MOD11C3-V6 Monthly at 5.6 km		The most significant warming trend in Alberta Canada was observed in May for both daytime and nighttime. In southern and southeastern parts of Alberta, daytime LST cooling occurred in July and August with slight nighttime warming in June and August. Significant daytime and nighttime cooling in November were observed in these regions.
[25]	Africa (2003-2017)	MOD11C3/MYD11C3 Monthly at 5.6 km		Northern and western Africa showed more significant warming LST trend than southern and eastern Africa. Winter warming was more significant in the western Africa. The most significant warming was around the equator and central Africa. In mid-north Africa, the daytime LST had an increasing trend.
[1]	India (2002-2022)	MOD11A1-V6.1 Daily at 1 km		LST has a declining trend in winter seasons while nighttime LST had an increasing trend in summer. Regions covered by snow or deserted regions followed by urban and semi-arid regions had highest daytime LST, while desert and urban regions had highest nighttime LST followed by semi-arid and forested regions.
[19]	Greenland (2001-2015)	MOD11A1-V6 Daily at 1 km		Summer warming was observed in populated areas. The MODIS LST trends were generally decreasing across Greenland.
[28]	Tibetan Plateau (2000-2017)	MOD11A1-V6 Daily at 1 km		Daytime and nighttime mean annual surface LST had an increasing trend. Elevation played in significant role in the daytime and nighttime LST, followed by NDVI in daytime and air temperature in nighttime.

TABLE II
SELECTED PUBLICATIONS ALONG WITH THEIR KEY FINDINGS FOR LANDSAT-DERIVED LST TRENDS, WHERE ALL THE PUBLICATIONS USED LINEAR REGRESSION FOR TREND ANALYSIS

Ref	Location & Period	Product & Resolution	Key findings
[83]	Sub-Shaharan Africa (1991-2013)	24 images, Landsat-5 TM, Landsat-7 ETM+, Landsat-8 OLI-TIRS, 30-120 m	Increased LST and urbanization trend were observed across the study region. Urbanized and built-up lands had a higher LST than green infrastructure areas.
[87]	India – Pune city (1990-2019)	8 images, Landsat-5 TM & Landsat-8 OLI-TIRS, 30-120 m	LST increased during summer and decreased during winter seasons since 1990. Daytime urban cool island was observed in the Pune city in both summer and winter as compared to its surrounding rural areas. The effect of LULC dynamics of seasonal LST was investigated.
[91]	USA – Las Vegas (1990-2010)	16-day Landsat-5 TM, 30 m	LST over new development regions in Las Vegas was decreasing during 1990-2010 because of an increase in vegetation cover in the form of golf course & parks.
[93]	Southeast Brazil (1985-2019)	14 images, Landsat-5 TM & Landsat-8 OLI-TIRS, 30-120 m	LST was increasing on bare soil during 1985-2019. LST was negatively correlated with moist in the wet season. Anthropogenic activity was an influential factor of warming trend in the study region.
[95]	Southern China (1991-2001)	3 images, Landsat-5 TM, 30 m	The change in construction materials in urban and vegetation dynamics in urban and rural areas were found to be correlated with LST dynamics. Urban and built-up lands increased while agricultural lands decreased. Urban areas showed a warming trend during 1991-2001.

E. Geostationary Instruments

TIR instruments of geostationary satellites, i.e., spinning enhanced visible and infrared imager (SEVIRI) and visible infrared spin scan radiometer (VISSR) onboard Geostationary Operational Environmental Satellite (NOAA's GOES), European Organisation for the Exploitation of Meteorological Satellites (EUMETSAT's) Meteosat Second Generation (ESA's MSG), and GMS-5 (Japanese Geostationary Meteorological Satellite, Himawari-5), respectively, were used in three studies in delineating LST trends [see Fig. 1(c)]. Underwood et al. [105] used GOES images-derived LST time series to map the evening cooling trends at 4-km spatial resolution in the Central Valley, USA, during 1997–2000. Oku et al. [106] used VISSR data at $0.1^\circ \times 0.1^\circ$ for mapping LST trends in the Tibetan Plateau and identified that the daily minimum had risen faster than the daily maximum during 1996–2002. Zhu et al. [107] utilized SEVIRI data at 1 km during 2010–2017 to observe LST variations following an earthquake in Iran.

IV. PMW-BASED STUDIES

Only one study used PMW instruments to delineate the LST trends, i.e., Special Sensor Microwave Imager (SSM/I), onboard polar-orbiting Defense Meteorological Satellite Program (DMSP) F-series satellites [108]. They used time series data over the Tibetan Plateau to quantify standardized LST anomalies (trends) during 1987–2008 and observed that annual and monthly LST decreased by 0.5° per decade with the highest at the Central Plateau.

V. OPPORTUNITIES AND CHALLENGES

Incorporating the variability of solar irradiance in the LST analysis is challenging, though the absolute value of total solar irradiance varies by 0.1% over the past two solar cycles [3], [109]. Performing trend analysis of any climate-related variables requires a continuous time series dataset over a longer period (typically 30 years or more). Some satellite constellations have already developed LST time series data over 30 years, such as the Landsat series, ESA, AVHRR, GOES, EUMETSAT, Himawari, and DMSP, except Terra/Aqua MODIS with 22 years. Though MODIS provides a bit shorter time series, however, its usages do not require additional preprocessing in analyzing LST trends. The design lifetime of a satellite, and its onboard instrument/s, is usually 15 years or much less. Therefore, constellations on different missions launch satellites with continuously improving instruments for better spatial and temporal coverage compared to previous generations. While continuity and improvements are important for a mission, it poses challenges to calibrating the data acquired by different instruments launched over time. It is extremely important to preprocess and harmonize the time series data so that the trends observed in the data will represent the real trends, not sensor-related or other artifacts. Due to the calibration-related challenges, we found a few studies that used observations from multiple instruments of a single mission or mixed instruments from multiple missions in delineating LST trends, rather than mostly using data from the same (or similar) instrument. Sections III and IV discuss both the opportunity and challenges of using TIR and PMW observations to delineate LST trends.

A. Polar-Orbiting TIR

In the polar-orbiting constellations, TIR instruments have the capacity to provide higher spatial resolution data, because

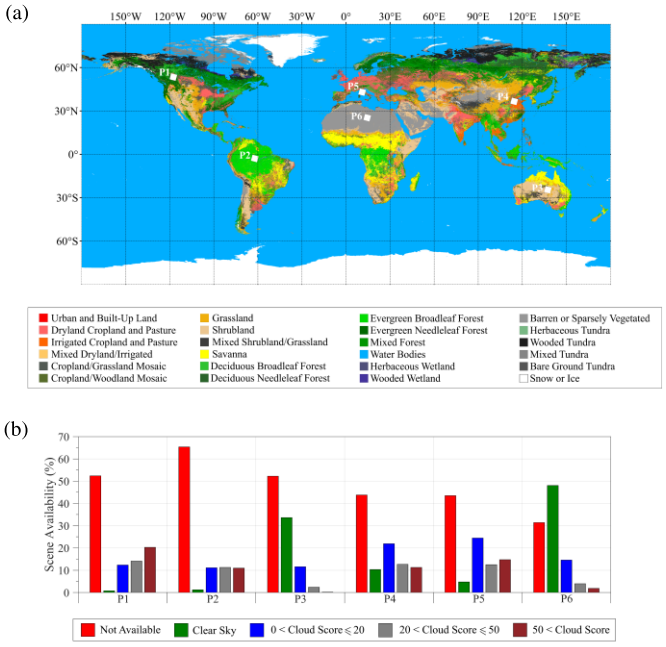

Fig. 2. (a) AVHRR-derived global LULC map showing six locations across the world with different climate and land cover characteristics—P1: mountains in North America; P2: forests in South America; P3: desert in Australia; P4: city in Asia; P5: mediterranean zone in Europe; and P6: desert in Africa. (b) Percentages of Landsat 5 TM scene availability for P1–P6 found in GEE. The cloud scores are between 0% (clear sky) and 100% (fully cloudy).

of acquiring shorter wavelengths, compared to the PMW instruments. Besides, TIR instruments onboard polar-orbiting satellites provide better spatial resolution than the geostationary satellites due to low-altitude orbits. However, atmospheric conditions, e.g., cloud presence, often pose major challenges in acquitting LST time series. While TIR is useful for weather applications such as cloud temperature and optical properties of clouds [110], cloud-contaminated pixels in the TIR bands are critical for its application in the LST trend analysis. Moreover, the availability of cloud-free data is limited for time series analysis, even in an arid/desert climate. For the understanding of available cloud-free data, we performed a search for Landsat 5 TM (the longest lifetime of a Landsat instrument over 1984–2013) image scenes using the Fmask algorithm through Google Earth Engine (GEE). The total numbers of available Landsat 5 TM scenes for six regions—P1–P6 (in different continents with different climates and land cover)—were 300, 218, 301, 354, 356, and 432, respectively, since 1984 (see Fig. 2). Considering the acquisition of a scene every 16 days during the lifetime of TM instrument, at least ~668 scenes should be available for each location. Moreover, the cloud-free (clear sky) scenes are much fewer in number among the available scenes, even in an arid region such as the Sahara Desert, Africa. Therefore, the limited availability of cloud-free data creates challenges for spatiotemporal analysis. Although such data gaps could be filled by applying appropriate gap-filling algorithm [111], it is potentially effective for removing small amount of cloud contamination, not the cloud-shadow effects. Another approach by NASA is to provide MODIS land products as LST composites of eight-day and monthly scales, prepared from the daily observations, to minimize cloud contamination. However, cloud-shadow pixels, including some clouds, may not be fully removed from the composites in many locations of the world. Despite the opportunities of using MODIS, noise usually affects the inversion errors strongly when the noise equivalent differential temperatures are used [112]. For instance, error bars indicated ±2 standard error for a 95% confidence interval in a monthly land temperature averaged in the Arctic during 2001–2020 from MODIS LST [113]. The good news is that the plankton, aerosol, cloud, ocean ecosystem (PACE), a NASA Earth-observing satellite mission, is scheduled to launch in 2024, where a highly advanced optical spectrometer (PACE's Ocean Color Instrument–OCI) will replace the aged MODIS [114].

NOAA's AVHRR, having the longest data records of the polar-orbiting TIR since 1979 with consistent spatial (1.1 km) and temporal (twice/day) resolutions, should probably the best option. However, we found a very limited number of studies in the literature since it would be quite challenging to generate well calibrated and harmonized time series observations of AVHRR instruments (AVHRR, AVHRR/2, and AVHRR/3) that were flown on 14 different platforms [115] because AVHRR sensors, onboard multiple platforms that have been active over the years, could have sensor degradation, scanline defects, satellite orbit drift, and channel calibration drift of the different AVHRRs [115]. Though a study successfully calibrated the observations of different AVHRR instruments during 1981–2015 over the peninsular Spain and determined the LST trends [116], however, such calibrated dataset across the globe is unavailable to our knowledge.

The Landsat series accumulated longer observations of TIR with a higher spatial resolution (60–120 m) since 1982, which also provides a better opportunity in delineating LST trends. The downside of using Landsat is its limited coverage on each scene (~182 × 185 km) compared to the AVHRR coverage (~6400 × 2400 km) and its temporal coverage of 16 days. To perform LST trends for a location, it is hard to find an appropriate number of cloud-free scenes over a season, even nearly impossible to get it for the same day in each year for a longer time series. We did not find, therefore, any global LST trends using Landsat TIR observations.

Another TIR instrument, namely, NASA's advanced spaceborne thermal emission and reflection radiometer (ASTER) has a similar observation period (since 2000) like MODIS with having 11 times higher spatial resolution (90 m) than MODIS, was not found in the literature for LST trend studies because it has: 1) small scene coverage, i.e., 60 × 60 km [117]; 2) not intended to continuously acquire data, and therefore, archived data are missing over time and space [117]; and 3) programed or acquired data were not free of cost from the beginning of the acquisition, which became freely available from April 1, 2016 [118].

B. Geostationary TIR

Geostationary satellite-based TIR observations have the opportunity of delineating LST trends at high temporal resolution (minutes to hours) with a reasonably high spatial resolution (2–6.9 km), because of having the longest observations in the remote sensing history, since 1975. However,

the challenges are related to cloud contamination issues, and the observations of each instrument do not cover the entire globe. Because of the objective of observing a targeted part of the globe, it became a challenge to delineate the LST trends from the geostationary TIR on a global scale.

C. Polar-Orbiting PMW

The PMW observations in the longer wavelengths could be a better choice (in comparison to TIR) for not having cloud contamination [110], which has been available since 1978 through the Scanning Multichannel Microwave Radiometer (SMMR) instrument onboard Nimbus-7 Pathfinder satellite. PMW observations have been available from different instruments, such as SMMR (1978–1987), SSM/I (1987–2020), and SSMIS (since 2004), Tropical Rainfall Measuring Mission (TRMM) Microwave Imager (TMI, onboard TRMM satellite from 1997 to 2015), Advanced Microwave Scanning Radiometer for Earth Observing System (AMSR-E, onboard Aqua from 2002 to 2011), Advanced Microwave Scanning Radiometer 2 (AMSR2, onboard global change observation mission-water1 (GCOM-W1) satellite since 2012), and Microwave Radiation Imager (MWRI, onboard FengYun-3 satellite series since 2008) [119]. Data of these satellites are available as brightness temperature from different data providers, such as SMMR, SSM/I, and ASMR-E from the National Snow and Ice Data Center (NSIDC), TMI from EARTHDATA, AMSR2 from the G-Portal address of Japan Aerospace Exploration Agency (JAXA), and MWRI from the Chinese National Satellite Meteorological Center (CNSMC). Combining the continuous PMW data from the constellations/missions shows a great opportunity in delineating LST trends at the global scale. However, LST retrieval from the PMW brightness temperature is considered quite challenging due to the following reasons.

1) It is hard to attain the atmospheric brightness temperature (downwelling) from the measured brightness temperature, surface emissivity, and decoupling the LST.
2) Atmospheric correction is challenging due to the strong variations of emissivity from surface properties (e.g., soil moisture, surface roughness, and vegetation cover) in the PMW region.
3) It additionally includes subsurface temperature instead of surface (skin) temperature only.
4) Validation of LST at the pixel level is difficult to realize [119].

Moreover, it provides coarser spatial resolution pixels (typically 25 × 25 km) than TIR data because it requires more area to cover on the ground in collecting a sufficient amount of low-frequency PMW energy reaching to the satellite sensors [120]. However, spatial resolution could be enhanced to all-weather (cloud contamination free) 1 km by a spatial-seamless PMW and TIR reconstruction method [121].

D. Cloud Computing and GEE

Recently, the feasibility of cloud computing for big data analytics through GEE, one of the most popular cloud computing systems, is explored in several studies (e.g., [1]). GEE has an interactive Web-based environment, where users can observe, analyze, or download various datasets. Users can develop their own code in Python or JavaScript for various applications and run it through GEE. Techniques, such as data fusion and cloud masking as well as machine learning algorithms, can also be performed through GEE, opening an opportunity for users to explore the available datasets and investigate spatiotemporal dynamics of LST, vegetation, land cover, and so on [122]. Due to its computing infrastructure, GEE can efficiently and rapidly handle big data and extensive computations [123].

VI. Research Gaps

In the annual LST trend analysis, different statistical methods (e.g., linear regression considering the parametric, and MK test and SSE for the nonparametric data) were applied to understand the patterns and magnitudes. These methods are applicable for any long-term time series data, either observations of weather stations or remote sensing. However, in the representation of annual trends, averaging the daily or monthly data to derive an annual value has an issue because it does not reflect the seasonal trends, either increasing (warming) or decreasing (cooling). Literature showed increasing trends during summer and decreasing trends during winter in many areas of the world. Once we average the data for a year, it neutralizes the seasonal patterns and trends and, thus, misses the true warming or cooling scenario for the area. For example, an area showed trends of $+1$ °C (increasing) and -1 °C (decreasing) during winter and summer, respectively, that certainly show no change in the annual trend. Therefore, we need to be cautious about presenting annual trends without looking into the seasonal trends. Since the issue is pervasive in nature, researcher should investigate different scenarios. For example, Shawky et al. [5] utilized the MODIS LST products and generated time series for each calendar month since 2000 at both pixel and ecoregion levels, and then, they applied the MK trend SEE methods to estimate daytime and nighttime LST gradients over South Asia. In this way, one can observe how the LST trend is changing for each calendar month since 2000. On the other hand, at an annual scale, i.e., the average of monthly LSTs for each year, one can only observe how the overall annual LST gradient changes over the years, though it also provides useful information. To obtain the annual LSTs, all the months should be considered or at least be estimated in case of missing LST values; otherwise, the annual LST values may get biased by seasonal variations, failing to provide a reliable annual gradient estimate.

Several studies reported daytime cooling (decreasing trends) and nighttime warming (increasing trends) estimated by the MODIS LST [41], [54], [74], [75] and discussed the possible rationales. However, the trends were not derived from the time series of daily maximum or minimum temperature. In a day cycle, either clear or overcast, the maximum and minimum LSTs during the daytime and nighttime are not synchronized with MODIS image acquisition times of 1:30 or 10:30 A.M. and 1:30 P.M. or 10:30 P.M., respectively. Although the Sun is at its highest point during noon when the Earth receives the most direct sunlight (incoming solar radiation), we do not get the maximum surface temperature at that time. The highest

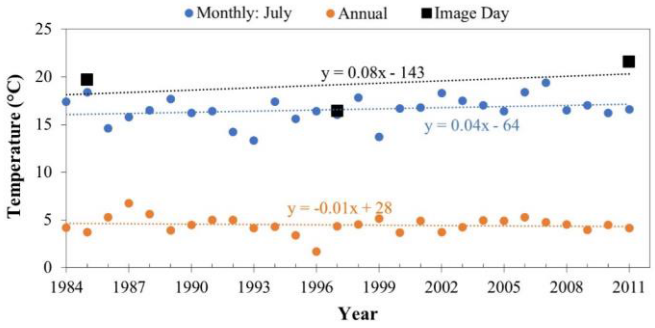

Fig. 3. Example of an erroneous LST trend estimation using three remote sensing images over a longer period of 1984–2011. The images were acquired on July 1, 1984, July 16, 1997, and July 31, 2011. The linear trends were calculated for temperature of the image dates, and mean temperatures of July and annual in the time series obtained from the Calgary International Airport site, where the data were available at free of cost from Environment Canada.

solar energy received and absorbed by the Earth's surface at noon starts to emit thermal energy that reaches the maximum in the afternoon, typically at 3–5 P.M. Inversely, the coldest time (i.e., the lowest temperature) of a daily cycle occurs sometime after sunrise when the speed at which the Earth's emitted thermal energy is no longer greater than the incoming solar radiation. Therefore, trends (such as daytime cooling and nighttime warming) estimated from the MODIS LST may require further investigation and should be noted with probable causes and explanations. However, the patterns of LST trends may not be impacted because the image acquisition time is consistent in the time series.

Some studies used a very small number of cloud-free images (e.g., two or three Landsat images) to analyze trends over 20 or 30 years, which may not provide the true trends. It is quite impossible to get cloud-free Landsat images acquired on the same day for all the years in a time series (see Fig. 2). Therefore, in the trend analysis, a very small number of cloud-free images were mostly used, having different acquisition dates in different years. One image might be taken in early summer for a year and others during the middle or end of summer for another year. Due to the location variability of the Earth toward the Sun, the changes in the magnitude of LST occur through the seasons, and even daily and monthly within a season. Seasons on the Earth are found in the temperate zones only, which extend from 23° 26′ to 66° 34′ latitudes in both northern and southern hemispheres. In these zones, we usually observe four seasons, spring, summer, fall (autumn), and winter, where each season is characterized by variations in temperature, precipitation, and daylight length [124]. The longer daylight (i.e., photoperiod) usually causes the contribution of more energy to the Earth's surface and thus higher air temperature and consequently higher LST.

Therefore, considering the variable energy over a season, LST trends derived from only a few images (acquired in different dates over a season in different years) could incorporate the seasonal change in the magnitude of trends, not the true temperature trends. An example case of such erroneous trend is presented in Fig. 3. The temperature trend from only three images over the period 1984–2011 was estimated 0.08 °C/yr. It was not a true trend for the station location because in situ observations showed the trends of −0.01 °C/yr and 0.04 °C/yr for annual and monthly (July), respectively (see Fig. 3). Hence, it is suggested to use as many images as possible over the time series, at least one image in every two to three years, and image dates as close as possible in the same month of a season.

In addition, it matters where a study area is, whether in the northern or southern hemisphere. It is because two hemispheres experience the seasons at different times of the year, and the daylight length, thus solar insolation (energy), varies with the latitudes. Therefore, researchers should be cautious when comparing the LST trends for different regions located in different hemispheres and latitudes to avoid any misrepresentation of the trends in LST.

VII. Future Research Potential

This article can be considered as a scope for conducting further studies to overcome the limitations and gaps for LST trend analysis. Research approaches would include developing methods of preparing a single calibrated dataset, with consistent data quality, from multiple instruments for the entire period of each constellation (mission). The seamless reconstruction of finer spatial resolution all-weather data in the entire world, using cloud contamination-free PMW at coarse and TIR at fine spatial resolution [121], would be another research direction. We could develop data fusion methods for the TIR observations of NOAA's AVHRR, MODIS, and Landsat [125] at the global scale, which would facilitate the longest time series LST data with an enhanced spatial resolution. Besides, to develop a consistent and finer spatial resolution over the history of remote sensing, data fusion of the observations in variable spatial resolution from different instruments in a constellation or across the constellations would be a major research opportunity.

Data fusion of AVHRR and MODIS observations would be the first choice due to having nearly similar spatial resolutions and, thus, likely to face less challenges. Furthermore, observations from the common period of instruments' operation, same mission or across missions, could be used for calibration and validation in developing a longer LST dataset. For example, ten years of AVHRR/3 observations could be calibrated with MODIS for a common period of 2000–2010, and observations (both AVHRR/3 and MODIS) of the remaining recent years could be used for validation. It would lead to developing a longer LST dataset since 1979 at 1.1 km from AVHRR observations. In the case of using a small number of images (e.g., Landsat scenes) with different acquisition dates for a longer period, innovative methods could be developed to standardize (normalize) each image of a year to be used in the time series.

More advanced trend analysis methods may also bypass the data availability limitation up to a certain level. For example, Ghaderpour et al. [126] and Ghaderpour [127] showed that the simultaneous season-trend fit models based on the least-squares spectral analysis has the potential of estimating trends more accurately in the presence of uncertainties due to atmospheric noise and missing data or gaps. For example, if LST data are available in certain months but limited in other

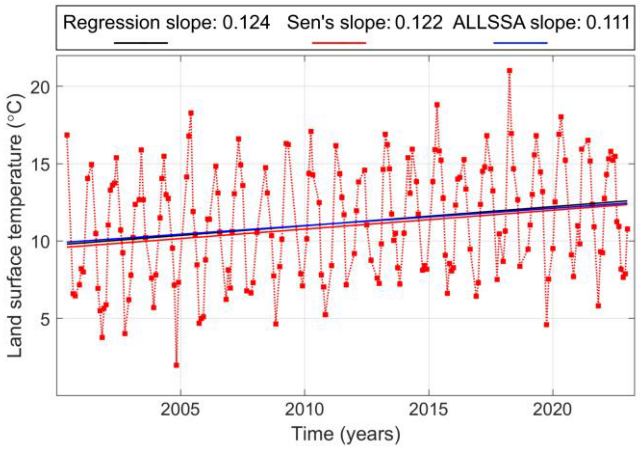

Fig. 4. Simulated LST time series with the trend fit results using linear regression, SSE, and ALLSSA. Note that ALLSSA also simultaneously estimated the seasonal component. All the trends are statistically significant at a 99% confidence level, and the actual slope is 0.1 °C/yr.

months, then the simultaneous season-trend fit model can better estimate the season and trend components, whereas the traditional regression methods may overestimate/underestimate the trend. For example, we simulated a set of LST time series using the following equation:

$$\mathrm{LST}(t) = T(t) + S(t) + E(t) \tag{1}$$

with $T(t) = b + mt$, $S(t) = A\sin(2\pi t)$, and $E(t) = \mathrm{wgn}(t, p)$, where b is the intercept, m is the slope, A is the amplitude, wgn is the white Gaussian noise, and p is the power of noise sample. Also, t is the time selected as monthly, i.e., the sampling rate is 12 samples per year. We applied the linear regression, MK test and its associated SSE, and anti-leakage least-squares spectral analysis (ALLSSA) to estimate the slope of such time series at a 99% confidence level.

The results for a case when $= 10$ °C, $m = 0.1$ °C/yr, and $A = 5$ °C with randomly eliminated 30% of the samples are shown in Fig. 4. The estimated slopes by linear regression, SEE, and ALLSSA are 0.124 °C/yr, 0.122 °C/yr, and 0.111 °C/yr, respectively. We performed this experiment on one million time series such that each time series was generated by (1), where the intercept, slope, and amplitude of the sinusoid were randomly generated for each time series and a random wgn was added to each time series. Then, up to 60% of samples were randomly selected and eliminated from each time series. The root-mean-square error (RMSE) was calculated for each method as

$$\mathrm{RMSE} = \sqrt{\frac{\sum_{i=1}^{N}\left(\hat{m}_i - m_i\right)^2}{N}} \tag{2}$$

where m_i is the simulated slope (the true value), $\hat{m}_i$ is the estimated slope, and N is the number of those estimated slopes that were statistically significant at a 99% confidence level. The RMSEs for the linear regression, SEE, and ALLSSA were 0.0314, 0.0307, and 0.0141, respectively, showing that the simultaneous season-trend fit model ALLSSA is superior in these cases.

Note that if $S(t)$ in (1) is the sum of multiple sinusoids of different amplitudes and frequencies and $T(t)$ is other types of trends such as quadratic or cubic, then ALLSSA can simultaneously estimate their coefficients with a high accuracy. The discussion above clearly shows that methods themselves can make a big difference in estimating LST trends, and thus, researchers should also be cautious about which techniques they apply to process their time series.

VIII. Conclusion

This article explored the opportunities and challenges of using remote sensing data, as well as potential research gaps in the methodological and conceptual approaches of utilizing the data. Understanding the extent and magnitude of the LST trend is important to cope with the ongoing climate change across the world. Using the appropriate remote sensing approaches, the mapping of temperature trends would help us in deciding the adaption and mitigation strategies for environmental sustainability. It would also direct local governments across the world to understand better about the warming trend in their jurisdiction that could help them act quickly and to address any potential negative risks posed by the warming.

References

[1] P. C. Pandey, A. Chauhan, and N. K. Maurya, "Evaluation of Earth observation datasets for LST trends over India and its implication in global warming," *Ecological Informat.*, vol. 72, Dec. 2022, Art. no. 101843, doi: 10.1016/j.ecoinf.2022.101843.

[2] L. Manzo-Delgado, R. Aguirre-Gómez, and R. Álvarez, "Multitemporal analysis of land surface temperature using NOAA-AVHRR: Preliminary relationships between climatic anomalies and forest fires," *Int. J. Remote Sens.*, vol. 25, no. 20, pp. 4417–4424, Oct. 2004, doi: 10.1080/01431160412331269643.

[3] J. D. Haigh, "The effects of solar variability on the Earth's climate," *Phil. Trans. Roy. Soc. London A, Math., Phys. Eng. Sci.*, vol. 361, no. 1802, pp. 95–111, Jan. 2003, doi: 10.1098/rsta.2002.1111.

[4] Y. Xu, Y. Shen, and Z. Wu, "Spatial and temporal variations of land surface temperature over the Tibetan plateau based on harmonic analysis," *Mountain Res. Develop.*, vol. 33, no. 1, pp. 85–94, Feb. 2013.

[5] M. Shawky et al., "Remote sensing-derived land surface temperature trends over South Asia," *Ecological Informat.*, vol. 74, May 2023, Art. no. 101969, doi: 10.1016/j.ecoinf.2022.101969.

[6] J. Mallick et al., "Spatiotemporal trends of temperature extremes in Bangladesh under changing climate using multi-statistical techniques," *Theor. Appl. Climatol.*, vol. 147, nos. 1–2, pp. 307–324, Jan. 2022, doi: 10.1007/S00704-021-03828-1.

[7] V. Masson-Delmotte et al., "IPCC AR6 summary for policymakers. In climate change 2021: The physical science basis. Contribution of working group I to the sixth assessment report of the intergovernmental panel on climate change," Work. Group 1, Cambridge Univ. Press, Cambridge, U.K., Tech. Rep. AR6, 2021.

[8] B. Song and K. Park, "Temperature trend analysis associated with land-cover changes using time series data (1980–2019) from 38 weather stations in South Korea," *Sustain. Cities Soc.*, vol. 65, pp. 1–14, Feb. 2021, doi: 10.1016/j.scs.2020.102615.

[9] M. Lepot, J.-B. Aubin, and F. Clemens, "Interpolation in time series: An introductive overview of existing methods, their performance criteria and uncertainty assessment," *Water*, vol. 9, no. 10, p. 796, Oct. 2017, doi: 10.3390/w9100796.

[10] J.-P. Chilès and P. Delfiner, *Geostatistics: Modeling Spatial Uncertainty*, 2nd ed. New York, NY, USA: Wiley, 2009.

[11] K. R. Rahaman and Q. K. Hassan, "Application of remote sensing to quantify local warming trends: A review," in *Proc. 5th Int. Conf. Informat., Electron. Vis. (ICIEV)*, May 2016, pp. 256–261.

[12] Q. K. Hassan, I. R. Ejiagha, M. R. Ahmed, A. Gupta, E. Rangelova, and A. Dewan, "Remote sensing of local warming trend in Alberta, Canada during 2001–2020, and its relationship with large-scale atmospheric circulations," *Remote Sens.*, vol. 13, pp. 1–21, Jul. 2021, doi: 10.3390/rs13173441.

[13] S. Liu, Y. Xie, H. Fang, H. Du, and P. Xu, "Trend test for hydrological and climatic time series considering the interaction of trend and autocorrelations," *Water*, vol. 14, no. 19, p. 3006, Sep. 2022, doi: 10.3390/w14193006.

[14] E. S. Vieira and J. A. N. F. Gomes, "A comparison of scopus and web of science for a typical university," *Scientometrics*, vol. 81, no. 2, pp. 587–600, Nov. 2009, doi: 10.1007/s11192-009-2178-0.

[15] Y. Li et al., "Potential and actual impacts of deforestation and afforestation on land surface temperature," *J. Geophys. Res. Atmos.*, vol. 121, pp. 14372–14386, Nov. 2016, doi: 10.1002/2016JD024969.

[16] M. Kilibarda et al., "Spatio-temporal interpolation of daily temperatures for global land areas at 1 km resolution," *J. Geophys. Res., Atmos.*, vol. 119, no. 5, pp. 2294–2313, Mar. 2014, doi: 10.1002/2013JD020803.

[17] K.-H. Tseng et al., "Satellite observed environmental changes over the Qinghai-Tibetan plateau," *Terr. Atmos. Ocean. Sci.*, vol. 22, pp. 229–239, Apr. 2011, doi: 10.3319/TAO.2010.09.17.03(TibXS).

[18] N. Wongsai, S. Wongsai, and A. R. Huete, "Annual seasonality extraction using the cubic spline function and decadal trend in temporal daytime MODIS LST data," *Remote Sens.*, vol. 9, pp. 1–17, Oct. 2017, doi: 10.3390/rs9121254.

[19] A. Westergaard-Nielsen, M. Karami, B. U. Hansen, S. Westermann, and B. Elberling, "Contrasting temperature trends across the ice-free part of Greenland," *Sci. Rep.*, vol. 8, no. 1, pp. 1–6, Jan. 2018, doi: 10.1038/s41598-018-19992-w.

[20] W. Zhao, J. He, Y. Wu, D. Xiong, F. Wen, and A. Li, "An analysis of land surface temperature trends in the central Himalayan region based on MODIS products," *Remote Sens.*, vol. 11, pp. 1–19, Jan. 2019, doi: 10.3390/rs11080983.

[21] Y. Liu et al., "Warming slowdown over the Tibetan plateau in recent decades," *Theor. Appl. Climatol.*, vol. 135, nos. 3–4, pp. 1375–1385, Feb. 2019, doi: 10.1007/s00704-018-2435-3.

[22] N. Pepin, H. Deng, H. Zhang, F. Zhang, S. Kang, and T. Yao, "An examination of temperature trends at high elevations across the Tibetan plateau: The use of MODIS LST to understand patterns of elevation-dependent warming," *J. Geophys. Research: Atmos.*, vol. 124, no. 11, pp. 5738–5756, Jun. 2019, doi: 10.1029/2018JD029798.

[23] B. Zhao et al., "A combined Terra and Aqua MODIS land surface temperature and meteorological station data product for China from 2003 to 2017," *Earth Syst. Sci. Data*, vol. 12, no. 4, pp. 2555–2577, Oct. 2020, doi: 10.5194/essd-12-2555-2020.

[24] S. Mal, S. Rani, and P. Maharana, "Estimation of spatio-temporal variability in land surface temperature over the Ganga river basin using MODIS data," *Geocarto Int.*, vol. 37, no. 13, pp. 3817–3839, Jul. 2022, doi: 10.1080/10106049.2020.1869331.

[25] N. NourEldeen, K. Mao, Z. Yuan, X. Shen, T. Xu, and Z. Qin, "Analysis of the spatiotemporal change in land surface temperature for a long-term sequence in Africa (2003–2017)," *Remote Sens.*, vol. 12, pp. 1–24, Feb. 2020, doi: 10.3390/rs12030488.

[26] Y. Qie, N. Wang, Y. Wu, and A. Chen, "Variations in winter surface temperature of the Purog Kangri ice field, Qinghai–Tibetan Plateau, 2001–2018, using MODIS data," *Remote Sens.*, vol. 2020, 12, 1-17, doi: 10.3390/rs12071133.

[27] Z. Song, H. Yang, X. Huang, W. Yu, J. Huang, and M. Ma, "The spatiotemporal pattern and influencing factors of land surface temperature change in China from 2003 to 2019," *Int. J. Appl. Earth Observ. Geoinf.*, vol. 104, pp. 1–11, Dec. 2021, doi: 10.1016/j.jag.2021.102537.

[28] M. Yang, W. Zhao, Q. Zhan, and D. Xiong, "Spatiotemporal patterns of land surface temperature change in the Tibetan plateau based on MODIS/Terra daily product from 2000 to 2018," *IEEE J. Sel. Topics Appl. Earth Observ. Remote Sens.*, vol. 14, pp. 6501–6514, 2021, doi: 10.1109/JSTARS.2021.3089851.

[29] W. Zhao, M. Yang, R. Chang, Q. Zhan, and Z. Li, "Surface warming trend analysis based on MODIS/Terra land surface temperature product at Gongga mountain in the southeastern Tibetan plateau," *J. Geophys. Res., Atmos.*, vol. 126, no. 22, pp. 1–26, Nov. 2021, doi: 10.1029/2020JD034205.

[30] I. Rousta, H. Olafsson, M. H. Nasserzadeh, H. Zhang, J. Krzyszczak, and P. Baranowski, "Dynamics of daytime land surface temperature (LST) variabilities in the middle east countries during 2001–2018," *Pure Appl. Geophys.*, vol. 178, no. 6, pp. 2357–2377, Jun. 2021, doi: 10.1007/s00024-021-02765-4.

[31] T. A. E. Prasetya, R. M. Devi, C. Fitrahanjani, T. Wahyuningtyas, and S. Muna, "Systematic assessment of the warming trend in Madagascar's mainland daytime land surface temperature from 2000 to 2019," *J. Afr. Earth Sci.*, vol. 189, pp. 1–9, May 2022, doi: 10.1016/j.jafrearsci.2022.104502.

[32] M. Munawar, T. A. E. Prasetya, R. McNeil, and R. Jani, "Statistical modeling for land surface temperature in Borneo island from 2000 to 2019," *Theor. Appl. Climatol.*, vol. 147, nos. 3–4, pp. 1627–1634, Feb. 2022, doi: 10.1007/s00704-021-03891-8.

[33] M. Castelli, "Evapotranspiration changes over the European Alps: Consistency of trends and their drivers between the MOD16 and SSEBop algorithms," *Remote Sens.*, vol. 13, pp. 1–34, Oct. 2021, doi: 10.3390/rs13214316.

[34] L. Olivera-Guerra, M. Quintanilla, I. Moletto-Lobos, E. Pichuante, C. Zamorano-Elgueta, and C. Mattar, "Water dynamics over a western Patagonian watershed: Land surface changes and human factors," *Sci. Total Environ.*, vol. 804, pp. 1–13, Jan. 2022, doi: 10.1016/j.scitotenv.2021.150221.

[35] R. Basu, G. Misra, and D. Sarkar, "A remote sensing based analysis of climate change in Sikkim supported by evidence from the field," *J. Mountain Sci.*, vol. 18, no. 5, pp. 1256–1267, May 2021, doi: 10.1007/s11629-020-6534-0.

[36] Q. Chi et al., "Quantifying the contribution of LUCC to surface energy budget: A case study of four typical cities in the yellow river basin in China," *Atmosphere*, vol. 12, pp. 1–20, Oct. 2021, doi: 10.3390/atmos12111374.

[37] P. Ji, X. Yuan, X. Liang, Y. Jiao, Y. Zhou, and Z. Liu, "High-resolution land surface modeling of the effect of long-term urbanization on hydrothermal changes over Beijing metropolitan area," *J. Geophys. Res., Atmos.*, vol. 126, no. 18, pp. 1–25, Sep. 2021, doi: 10.1029/2021JD034787.

[38] A. A. Jamali, R. G. Kalkhajeh, T. O. Randhir, and S. He, "Modeling relationship between land surface temperature anomaly and environmental factors using GEE and Giovanni," *J. Environ. Manage.*, vol. 302, pp. 1–10, Jan. 2022, doi: 10.1016/j.jenvman.2021.113970.

[39] R. Lemoine-Rodríguez, L. Inostroza, and H. Zepp, "Does urban climate follow urban form? Analysing intraurban LST trajectories versus urban form trends in 3 cities with different background climates," *Sci. Total Environ.*, vol. 830, pp. 1–13, 2022, doi: 10.1016/j.scitotenv.2022.154570.

[40] M. Panwar, A. Agarwal, and V. Devadas, "Analyzing land surface temperature trends using non-parametric approach: A case of Delhi, India," *Urban Climate*, vol. 24, pp. 19–25, Jun. 2018, doi: 10.1016/j.uclim.2018.01.003.

[41] H. S. Sussman, A. Raghavendra, and L. Zhou, "Impacts of increased urbanization on surface temperature, vegetation, and aerosols over Bengaluru, India," *Remote Sens. Appl., Soc. Environ.*, vol. 16, pp. 1–12, Nov. 2019, doi: 10.1016/j.rsase.2019.100261.

[42] S. Raj, S. K. Paul, A. Chakraborty, and J. Kuttippurath, "Anthropogenic forcing exacerbating the urban heat islands in India," *J. Environ. Manage.*, vol. 257, Mar. 2020, Art. no. 110006, doi: 10.1016/j.jenvman.2019.110006.

[43] T. Ren, W. Zhou, and J. Wang, "Beyond intensity of urban heat island effect: A continental scale analysis on land surface temperature in major Chinese cities," *Sci. Total Environ.*, vol. 791, Oct. 2021, Art. no. 148334, doi: 10.1016/j.scitotenv.2021.148334.

[44] N. Benas, N. Chrysoulakis, and C. Cartalis, "Trends of urban surface temperature and heat island characteristics in the Mediterranean," *Theor. Appl. Climatol.*, vol. 130, nos. 3–4, pp. 807–816, Nov. 2017, doi: 10.1007/s00704-016-1905-8.

[45] P. Mohammad, A. Goswami, and S. Bonafoni, "The impact of the land cover dynamics on surface urban heat island variations in semi-arid cities: A case study in Ahmedabad city, India, using multi-sensor/source data," *Sensors*, vol. 19, Jul. 2019, p. 3701, doi: 10.3390/s19173701.

[46] A. Dewan, G. Kiselev, D. Botje, G. I. Mahmud, M. H. Bhuian, and Q. K. Hassan, "Surface urban heat island intensity in five major cities of Bangladesh: Patterns, drivers and trends," *Sustain. Cities Soc.*, vol. 71, Aug. 2021, Art. no. 102926, doi: 10.1016/j.scs.2021.102926.

[47] Y. Lu, J. Yang, and S. Ma, "Dynamic changes of local climate zones in the Guangdong–Hong Kong–Macao greater bay area and their spatio-temporal impacts on the surface urban heat island effect between 2005 and 2015," *Sustainability*, vol. 2021, 13, pp. 1–20, doi: 10.3390/su13116374.

[48] A. Siddiqui, G. Kushwaha, B. Nikam, S. K. Srivastav, A. Shelar, and P. Kumar, "Analysing the day/night seasonal and annual changes and trends in land surface temperature and surface urban heat island intensity (SUHII) for Indian cities," *Sustain. Cities Soc.*, vol. 75, Dec. 2021, Art. no. 103374, doi: 10.1016/j.scs.2021.103374.

[49] I. R. Ejiagha, M. R. Ahmed, A. Dewan, A. Gupta, E. Rangelova, and Q. K. Hassan, "Urban warming of the two most populated cities in the Canadian province of Alberta, and its influencing factors," *Sensors*, vol. 22, p. 2894, Mar. 2022, doi: 10.3390/s22082894.

[50] R. Lemoine-Rodríguez, L. Inostroza, and H. Zepp, "Intraurban heterogeneity of space-time land surface temperature trends in six climate-diverse cities," *Sci. Total Environ.*, vol. 804, Jan. 2022, Art. no. 150037, doi: 10.1016/j.scitotenv.2021.150037.

[51] Y. Hu, G. Jia, M. Hou, X. Zhang, F. Zheng, and Y. Liu, "The cumulative effects of urban expansion on land surface temperatures in metropolitan Jing-Jin-Tang, China," *J. Geophys. Res. Atmos.*, vol. 120, pp. 9932–9943, Oct. 2015, doi: 10.1002/.2015JD023653.

[52] J. Muro et al., "Land surface temperature trends as indicator of land use changes in wetlands," *Int. J. Appl. Earth Observ. Geoinf.*, vol. 70, pp. 62–71, Aug. 2018, doi: 10.1016/j.jag.2018.02.002.

[53] T. Liu, L. Yu, and S. Zhang, "Impacts of wetland reclamation and paddy field expansion on observed local temperature trends in the Sanjiang plain of China," *J. Geophys. Res., Earth Surf.*, vol. 124, no. 2, pp. 414–426, Feb. 2019, doi: 10.1029/2018JF004846.

[54] L. Yu and T. Liu, "The impact of artificial wetland expansion on local temperature in the growing season—The case study of the Sanjiang plain, China," *Remote Sens.*, vol. 11, p. 2915, Dec. 2019, doi: 10.3390/rs11242915.

[55] F. O. Akinyemi, M. Ikanyeng, and J. Muro, "Land cover change effects on land surface temperature trends in an African urbanizing dryland region," *City Environ. Interact.*, vol. 4, Dec. 2019, Art. no. 100029, doi: 10.1016/j.cacint.2020.100029.

[56] A. Suwanwong and N. Kongchouy, "Cubic spline regression model and gee for land surface temperature trend using modis in the cloud forest of Khao Nan national park southern Thailand during 2000–2015," *J. Eng. Appl. Sci.*, vol. 11, no. 11, pp. 2387–2395, 2016. [Online]. Available: https://medwelljournals.com/abstract/?doi=jeasci.2016.2387.2395

[57] J. Tao et al., "Elevation-dependent temperature change in the Qinghai–Xizang plateau grassland during the past decade," *Theor. Appl. Climatol.*, vol. 117, nos. 1–2, pp. 61–71, Jul. 2014, doi: 10.1007/s00704-013-0976-z.

[58] J. Aguilar-Lome, R. Espinoza-Villar, J.-C. Espinoza, J. Rojas-Acuña, B. L. Willems, and W.-M. Leyva-Molina, "Elevation-dependent warming of land surface temperatures in the Andes assessed using MODIS LST time series (2000–2017)," *Int. J. Appl. Earth Observ. Geoinf.*, vol. 77, pp. 119–128, May 2019, doi: 10.1016/j.jag.2018.12.013.

[59] M. Zhang et al., "Creating new near-surface air temperature datasets to understand elevation-dependent warming in the Tibetan plateau," *Remote Sens.*, vol. 12, p. 1722, Apr. 2020, doi: 10.3390/rs12111722.

[60] Z. Song, S. Liang, L. Feng, T. He, X.-P. Song, and L. Zhang, "Temperature changes in three Gorges reservoir area and linkage with three Gorges project," *J. Geophys. Res., Atmos.*, vol. 122, no. 9, pp. 4866–4879, May 2017, doi: 10.1002/2016JD025978.

[61] K. Adepoju, S. Adelabu, and O. Fashae, "Vegetation response to recent trends in climate and landuse dynamics in a typical humid and dry tropical region under global change," *Adv. Meteorol.*, vol. 2019, pp. 1–15, Dec. 2019, doi: 10.1155/2019/4946127.

[62] P. Fu, "Responses of vegetation productivity to temperature trends over continental United States from MODIS imagery," *IEEE J. Sel. Topics Appl. Earth Observ. Remote Sens.*, vol. 12, no. 4, pp. 1085–1090, Apr. 2019, doi: 10.1109/JSTARS.2019.2903080.

[63] H. Hallang, S. O. Los, and J. F. Hiemstra, "Permafrost, thermal conditions and vegetation patterns since the mid-20th century: A remote sensing approach applied to Jotunheimen, Norway," *Prog. Phys. Geogr. Earth Environ.*, vol. 46, no. 5, pp. 716–736, May 2022, doi: 10.25384/SAGE.c.5984834.v1.

[64] E. Heck, K. M. de Beurs, B. C. Owsley, and G. M. Henebry, "Evaluation of the MODIS collections 5 and 6 for change analysis of vegetation and land surface temperature dynamics in north and south America," *ISPRS J. Photogramm. Remote Sens.*, vol. 156, pp. 121–134, Oct. 2019, doi: 10.1016/j.isprsjprs.2019.07.011.

[65] N. Nandkeolyar and G. S. Kiran, "A climatological study of the spatio-temporal variability of land surface temperature and vegetation cover of vadodara district of Gujarat using satellite data," *Int. J. Remote Sens.*, vol. 40, no. 1, pp. 218–236, Jan. 2019, doi: 10.1080/01431161.2018.1512766.

[66] V. A. Olivares-Contreras, C. Mattar, A. G. Gutiérrez, and J. C. Jiménez, "Warming trends in Patagonian subantartic forest," *Int. J. Appl. Earth Observ. Geoinf.*, vol. 76, pp. 51–65, Apr. 2019, doi: 10.1016/j.jag.2018.10.015.

[67] R. S. Vilanova et al., "Past and future assessment of vegetation activity for the state of Amazonas-Brazil," *Remote Sens. Appl., Soc. Environ.*, vol. 17, Jan. 2020, Art. no. 100278, doi: 10.1016/j.rsase.2019.100278.

[68] L. Wang, N. Guo, S. Sha, Y. Yang, X. Wang, and D. Hu, "Effects of land cover type conversion on water exchange and climate change in the source area of the yellow river," *Theor. Appl. Climatol.*, vol. 149, nos. 1–2, pp. 525–536, Jul. 2022, doi: 10.1007/s00704-022-04065-w.

[69] B. Wei, Y. Bao, S. Yu, S. Yin, and Y. Zhang, "Analysis of land surface temperature variation based on MODIS data a case study of the agricultural pastural ecotone of northern China," *Int. J. Appl. Earth Observ. Geoinf.*, vol. 100, pp. 1–14, Aug. 2021, doi: 10.1016/j.jag.2021.102342.

[70] H. Lu and J. Shi, "Reconstruction and analysis of temporal and spatial variations in surface soil moisture in China using remote sensing," *Chin. Sci. Bull.*, vol. 57, no. 22, pp. 2824–2834, Aug. 2012, doi: 10.1007/s11434-012-5011-8.

[71] A. G. Dhorde and N. R. Patel, "Spatio-temporal variation in terminal drought over western India using dryness index derived from long-term MODIS data," *Ecological Informat.*, vol. 32, pp. 28–38, Mar. 2016, doi: 10.1016/j.ecoinf.2015.12.007.

[72] R. Jafari and M. Abedi, "Remote sensing-based biological and nonbiological indices for evaluating desertification in iran: Image versus field indices," *Land Degradation Develop.*, vol. 32, no. 9, pp. 2805–2822, May 2021, doi: 10.1002/ldr.3958.

[73] L. Zhou, Y. Tian, S. Baidya Roy, C. Thorncroft, L. F. Bosart, and Y. Hu, "Impacts of wind farms on land surface temperature," *Nature Climate Change*, vol. 2, no. 7, pp. 539–543, Jul. 2012, doi: 10.1038/nclimate1505.

[74] R. Chang, R. Zhu, and P. Guo, "A case study of land-surface-temperature impact from large-scale deployment of wind farms in China from Guazhou," *Remote Sens.*, vol. 8, p. 790, Sep. 2016, doi: 10.3390/rs8100790.

[75] L. Luo et al., "Local climatic and environmental effects of an onshore wind farm in North China," *Agricult. Forest Meteorol.*, vols. 308–309, Oct. 2021, Art. no. 108607, doi: 10.1016/j.agrformet.2021.108607.

[76] W. Zhao, J. He, G. Yin, F. Wen, and H. Wu, "Spatiotemporal variability in land surface temperature over the mountainous region affected by the 2008 Wenchuan earthquake from 2000 to 2017," *J. Geophys. Res., Atmos.*, vol. 124, no. 4, pp. 1975–1991, Feb. 2019, doi: 10.1029/2018JD030007.

[77] J. Zhao, S. Zhang, K. Yang, Y. Zhu, and Y. Ma, "Spatio-temporal variations of CO_2 emission from energy consumption in the Yangtze river delta region of China and its relationship with nighttime land surface temperature," *Sustainability*, vol. 12, pp. 1–17, Oct. 2020, doi: 10.3390/su12208388.

[78] J. Longbottom, C. Caminade, H. S. Gibson, D. J. Weiss, S. Torr, and J. S. Lord, "Modelling the impact of climate change on the distribution and abundance of tsetse in northern Zimbabwe," *Parasites Vectors*, vol. 13, no. 1, pp. 1–11, Dec. 2020, doi: 10.1186/s13071-020-04398-3.

[79] X. Qiu, L. Zhang, L. Wenliang, Y. Yang, and P. Tao, "Studies on changes and cause of the minimum air temperature in songnen plain of China during 1961–2010," *Acta Ecologica Sinica*, vol. 36, no. 5, pp. 311–320, Oct. 2016, doi: 10.1016/j.chnaes.2016.06.009.

[80] T. A. Abera, J. Heiskanen, E. E. Maeda, and P. K. E. Pellikka, "Land surface temperature trend and its drivers in east Africa," *J. Geophys. Res., Atmos.*, vol. 125, no. 23, pp. 1–18, Dec. 2020, doi: 10.1029/2020JD033446.

[81] Y. Yan et al., "Driving forces of land surface temperature anomalous changes in north America in 2002–2018," *Sci. Rep.*, vol. 10, no. 1, pp. 1–13, Apr. 2020, doi: 10.1038/s41598-020-63701-5.

[82] H. Ebrahimy, H. Aghighi, M. Azadbakht, M. Amani, S. Mahdavi, and A. A. Matkan, "Downscaling MODIS land surface temperature product using an adaptive random forest regression method and Google Earth engine for a 19-years spatiotemporal trend analysis over Iran," *IEEE J. Sel. Topics Appl. Earth Observ. Remote Sens.*, vol. 14, pp. 2103–2112, 2021, doi: 10.1109/JSTARS.2021.3051422.

[83] N. Di Leo, F. J. Escobedo, and M. Dubbeling, "The role of urban green infrastructure in mitigating land surface temperature in Bobo-Dioulasso, Burkina Faso," *Environ., Develop. Sustainability*, vol. 18, no. 2, pp. 373–392, Apr. 2016, doi: 10.1007/s10668-015-9653-y.

[84] A. Rasul, H. Balzter, and C. Smith, "Applying a normalized ratio scale technique to assess influences of urban expansion on land surface temperature of the semi-arid city of Erbil," *Int. J. Remote Sens.*, vol. 38, no. 13, pp. 3960–3980, Jul. 2017, doi: 10.1080/01431161.2017.1312030.

[85] L. Wang, Y. Yao, and S. Zhang, "A quantitative analysis of urban water landscape pattern changes and their impacts on surface temperatures," *Fresenius Environ. Bull.*, vol. 25, pp. 5194–5201, Jan. 2016.

[86] R. Aabeyir, K. Peprah, and K. O. Hackman, "Spatio-temporal pattern of urban vegetation in the central business district of the Wa municipality of Ghana," *Trees, Forests People*, vol. 8, Jun. 2022, Art. no. 100261, doi: 10.1016/j.tfp.2022.100261.

[87] K. J. Gohain, P. Mohammad, and A. Goswami, "Assessing the impact of land use land cover changes on land surface temperature over Pune city, India," *Quaternary Int.*, vol. 2021, pp. 575–576, 259-269, doi: 10.1016/j.quaint.2020.04.052.

[88] S. Tayebi, H. Mohammadi, A. Shamsipoor, S. Tayebi, S. A. Alavi, and S. Hoseinioun, "Analysis of land surface temperature trend and climate resilience challenges in Tehran," *Int. J. Environ. Sci. Technol.*, vol. 16, no. 12, pp. 8585–8594, Dec. 2019, doi: 10.1007/s13762-019-02329-z.

[89] S. Ongsomwang, S. Dasananda, and W. Prasomsup, "Spatio-temporal urban heat island phenomena assessment using landsat imagery: A case study of Bangkok metropolitan and its Vicinity, Thailand," *Environ. Natural Resour. J.*, vol. 16, pp. 29–44, Dec. 2018, doi: 10.14456/ennrj.2018.13.

[90] R. Renteria, S. Grineski, T. Collins, A. Flores, and S. Trego, "Social disparities in neighborhood heat in the Northeast United States," *Environ. Res.*, vol. 203, Jan. 2022, Art. no. 111805, doi: 10.1016/j.envres.2021.111805.

[91] H. Stephen, "Trend analysis of Las Vegas land cover and temperature using remote sensing," *Land*, vol. 7, pp. 1–19, Nov. 2018, doi: 10.3390/land7040135.

[92] R. Jafari and S. Hasheminasab, "Assessing the effects of dam building on land degradation in central Iran with landsat LST and LULC time series," *Environ. Monitor. Assessment*, vol. 189, no. 2, pp. 1–15, Feb. 2017, doi: 10.1007/s10661-017-5792-y.

[93] V. M. Sayão et al., "Land use/land cover changes and bare soil surface temperature monitoring in southeast Brazil," *Geoderma Regional*, vol. 22, Sep. 2020, Art. no. e00313, doi: 10.1016/j.geodrs.2020.e00313.

[94] K. Anjali and T. Roshni, "Linking satellite-based forest cover change with rainfall and land surface temperature in kerala, India," *Environ., Develop. Sustainability*, vol. 24, no. 9, pp. 11282–11300, Sep. 2022, doi: 10.1007/s10668-021-01908-w.

[95] H. Xiao and Q. Weng, "The impact of land use and land cover changes on land surface temperature in a Karst area of China," *J. Environ. Manage.*, vol. 85, pp. 245–257, Oct. 2007, doi: 10.1016/j.jenvman.2006.07.016.

[96] R. Jiang, Y. Zhang, L. Chen, W. Xiang, G. Liu, and H. Zheng, "The spatio-temporal characteristics of land surface temperatures in Shanghai, and their responses to land-use change," *J. Environ. Accounting Manage.*, vol. 2, no. 3, pp. 217–228, Sep. 2014, doi: 10.5890/JEAM.2014.09.003.

[97] R. Sharma, A. Chakraborty, and P. K. Joshi, "Geospatial quantification and analysis of environmental changes in urbanizing city of Kolkata (India)," *Environ. Monitor. Assessment*, vol. 187, no. 1, pp. 1–12, Jan. 2015, doi: 10.1007/s10661-014-4206-7.

[98] K. McConnell et al., "A quasi-experimental approach for evaluating the heat mitigation effects of green roofs in Chicago, Illinois," *Sustain. Cities Soc.*, vol. 76, Jan. 2022, Art. no. 103376, doi: 10.1016/j.scs.2021.103376.

[99] B. Reyes, T. Hogue, and R. Maxwell, "Urban irrigation suppresses land surface temperature and changes the hydrologic regime in semi-arid regions," *Water*, vol. 10, p. 1563, Nov. 2018, doi: 10.3390/w10111563.

[100] N. Lu et al., "Hierarchical Bayesian space-time estimation of monthly maximum and minimum surface air temperature," *Remote Sens. Environ.*, vol. 211, pp. 48–58, Jun. 2018, doi: 10.1016/j.rse.2018.04.006.

[101] X. Ouyang, D. Chen, Y. Feng, and Y. Lei, "Comparison of seasonal surface temperature trend, spatial variability, and elevation dependency from satellite-derived products and numerical simulations over the Tibetan plateau from 2003 to 2011," *Int. J. Remote Sens.*, vol. 40, nos. 5–6, pp. 1844–1857, Mar. 2019, doi: 10.1080/01431161.2018.1482024.

[102] X. Ouyang, D. Chen, S. B. Duan, Y. Lei, Y. Dou, and G. Hu, "Validation and analysis of long-term AATSR land surface temperature product in the Heihe River basin, China," *Remote Sens.*, vol. 9, no. 2, p. 152, 2017, doi: 10.3390/rs9020152.

[103] U. S. Bhatt et al., "Changing seasonality of panarctic Tundra vegetation in relationship to climatic variables," *Environ. Res. Lett.*, vol. 12, pp. 1–17, May 2017, doi: 10.1088/1748-9326/aa6b0b.

[104] A. C. T. Pinheiro, R. Mahoney, J. L. Privette, and C. J. Tucker, "Development of a daily long term record of NOAA-14 AVHRR land surface temperature over Africa," *Remote Sens. Environ.*, vol. 103, no. 2, pp. 153–164, Jul. 2006, doi: 10.1016/j.rse.2006.03.009.

[105] S. J. Underwood, G. P. Ellrod, and A. L. Kuhnert, "A multiple-case analysis of nocturnal radiation-fog development in the central valley of California utilizing the GOES nighttime fog product," *J. Appl. Meteorol.*, vol. 43, pp. 297–311, Feb. 2004, doi: 10.1175/1520-0450(2004)043<0297:AMAONR>2.0.CO;2.

[106] Y. Oku, H. Ishikawa, S. Haginoya, and Y. Ma, "Recent trends in land surface temperature on the Tibetan plateau," *J. Climate*, vol. 19, no. 12, pp. 2995–3003, Jun. 2006, doi: 10.1175/JCLI3811.1.

[107] C. Zhu, Z. Jiao, X. Shan, G. Zhang, and Y. Li, "Land surface temperature variation following the 2017 Mw 7.3 Iran earthquake," *Remote Sens.*, vol. 11, pp. 1–13, Oct. 2019, doi: 10.3390/rs11202411.

[108] M. S. Salama, R. Van Der Velde, L. Zhong, Y. Ma, M. Ofwono, and Z. Su, "Decadal variations of land surface temperature anomalies observed over the Tibetan plateau by the special sensor microwave imager (SSM/I) from 1987 to 2008," *Climatic Change*, vol. 114, nos. 3–4, pp. 769–781, Oct. 2012, doi: 10.1007/s10584-012-0427-3.

[109] T. Phillips, *Solar Variability and Terrestrial Climate. Global Climate Change: Vital Signs of the Planet*. Accessed: Jan. 12, 2013. [Online]. Available: https://climate.nasa.gov/news/849/solar-variability-and-terrestrial-climate/

[110] C. J. Tomlinson, L. Chapman, J. E. Thornes, and C. Baker, "Remote sensing land surface temperature for meteorology and climatology: A review," *Meteorological Appl.*, vol. 18, no. 3, pp. 296–306, Sep. 2011, doi: 10.1002/met.287.

[111] E. H. Chowdhury and Q. K. Hassan, "Use of remote sensing-derived variables in developing a forest fire danger forecasting system," *Natural Hazards*, vol. 67, no. 2, pp. 321–334, Jun. 2013, doi: 10.1007/s11069-013-0564-7.

[112] H. Shao, C. Liu, C. Li, J. Wang, and F. Xie, "Temperature and emissivity inversion accuracy of spectral parameter changes and noise of hyperspectral thermal infrared imaging spectrometers," *Sensors*, vol. 20, no. 7, p. 2109, Apr. 2020, doi: 10.3390/s20072109.

[113] Y.-R. Wang, D. O. Hessen, B. H. Samset, and F. Stordal, "Evaluating global and regional land warming trends in the past decades with both MODIS and ERA5-land land surface temperature data," *Remote Sens. Environ.*, vol. 280, Oct. 2022, Art. no. 113181, doi: 10.1016/j.rse.2022.113181.

[114] *National Aeronautics and Space Administration. Get to Know PACE: Plankton, Aerosol, Cloud, Ocean Ecosystem*. Accessed: Jan. 12, 2023. [Online]. Available: https://pace.oceansciences.org/about.htm

[115] S. Dech et al., "Potential and challenges of harmonizing 40 years of AVHRR data: The TIMELINE experience," *Remote Sens.*, vol. 13, pp. 1–35, Sep. 2021, doi: 10.3390/rs13183618.

[116] M. Khorchani et al., "Trends in LST over the peninsular Spain as derived from the AVHRR imagery data," *Global Planet. Change*, vol. 166, pp. 75–93, Jul. 2018, doi: 10.1016/j.gloplacha.2018.04.006.

[117] M. Abrams, S. Hook, and B. Ramachandran, "ASTER user handbook," Jet Propuls. Lab. (JPL), Pasadena, CA, USA, and EROS Data Center, Sioux Falls, SD, USA, Version 2, Tech. Rep., 2002.

[118] *USGS: LPDAAC is There a Fee Associated With Ordering ASTER Data?* Accessed: Dec. 17, 2021. [Online]. Available: https://lpdaac.usgs.gov/resources/faqs/

[119] S. B. Duan et al., "Land surface temperature retrieval from passive microwave satellite observations: State-of-the-art and future directions," *Remote Sens.*, vol. 12, p. 2573, Aug. 2020, doi: 10.3390/RS12162573.

[120] K. Jensen and K. Mcdonald, "Surface water microwave product series version 3: A near-real time and 25-year historical global inundated area fraction time series from active and passive microwave remote sensing," *IEEE Geosci. Remote Sens. Lett.*, vol. 16, no. 9, pp. 1402–1406, Sep. 2019, doi: 10.1109/LGRS.2019.2898779.

[121] X. Zhang, J. Zhou, S. Liang, L. Chai, D. Wang, and J. Liu, "Estimation of 1-km all-weather remotely sensed land surface temperature based on reconstructed spatial-seamless satellite passive microwave brightness temperature and thermal infrared data," *ISPRS J. Photogramm. Remote Sens.*, vol. 167, pp. 321–344, Sep. 2020, doi: 10.1016/j.isprsjprs.2020.07.014.

[122] A. T. Dehkordi, M. J. V. Zoej, H. Ghasemi, E. Ghaderpour, and Q. K. Hassan, "A new clustering method to generate training samples for supervised monitoring of long-term water surface dynamics using landsat data through Google Earth engine," *Sustainability*, vol. 14, no. 13, p. 8046, Jun. 2022, doi: 10.3390/su14138046.

[123] M. Waleed and M. Sajjad, "Leveraging cloud-based computing and spatial modeling approaches for land surface temperature disparities in response to land cover change: Evidence from Pakistan," *Remote Sens. Appl., Soc. Environ.*, vol. 25, Jan. 2022, Art. no. 100665, doi: 10.1016/j.rsase.2021.100665.

[124] G. O. Abell, D. Morrison, and S. C. Wolff, *Exploration of the Universe*, 6th ed. Rochester, NY, USA: Saunders College, 1993.

[125] K. Hazaymeh and Q. K. Hassan, "Fusion of MODIS and Landsat-8 surface temperature images: A new approach," *PLoS ONE*, vol. 10, no. 3, Mar. 2015, Art. no. e0117755, doi: 10.1371/journal.pone.0117755.

[126] E. Ghaderpour, T. Vujadinovic, and Q. K. Hassan, "Application of the least-squares wavelet software in hydrology: Athabasca river basin," *J. Hydrol., Regional Stud.*, vol. 36, Aug. 2021, Art. no. 100847, doi: 10.1016/j.ejrh.2021.100847.

[127] E. Ghaderpour, "JUST: MATLAB and Python software for change detection and time series analysis," *GPS Solutions*, vol. 25, no. 3, p. 85, Jul. 2021, doi: 10.1007/s10291-021-01118-x.

M. Razu Ahmed received the M.A. degree in geography from Brock University, St. Catharines, ON, Canada, in 2016, and the Ph.D. degree in geomatics engineering from the University of Calgary, Calgary, AB, Canada, in 2020.

He is currently a Postdoctoral Associate with the University of Calgary. His current research interests include wildland-urban interface fire, forecasting forest fire, natural hazards/disasters, local warming, and dynamics of land surface temperature (LST) using Earth-observing satellites, remote sensing and geographic information system (GIS), environmental modeling, and integrated GIScience approaches.

Ebrahim Ghaderpour received the first Ph.D. degree in theoretical and computational science from the University of Lethbridge, Lethbridge, AB, Canada, in 2014, and the second Ph.D. degree in Earth and space science from York University, Toronto, ON, Canada, in 2018.

He completed two postdoctoral appointments at the Department of Mathematics and Statistics and the Department of Geomatics Engineering, University of Calgary, Calgary, AB. He is currently an Assistant Professor with the Department of Earth Sciences, Sapienza University of Rome, Rome, Italy, and the CEO of Earth and Space Inc., Calgary. His current research interests include big data analytics and time series analysis with applications in various fields, such as remote sensing, geology, geophysics, astronomy, finance, and medicine.

Anil Gupta received the Ph.D. degree in civil/water resource engineering from the Asian Institute of Technology, Klong Luang, Pathum Thani, Thailand, in 1995.

He is a Director of Alberta Environment and Protection Areas, Calgary, AB, Canada. His current research interests include hydrological modeling, climate change, water resource and watershed managements, water surface, and environmental monitoring and assessment.

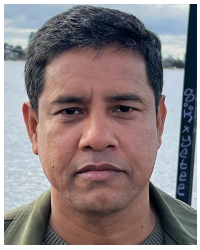

Ashraf Dewan received the Ph.D. degree in environmental science and technology from Okayama University, Tsushima-Naka, Okayama, Japan, in 2005.

He is an Associate Professor with the School of Earth and Planetary Sciences, Curtin University, Perth, WA, Australia. His current research interests include the application of geospatial intelligence to the study of urban climate, health geography, climate services, disaster risk reduction, and climate risk management.

Quazi K. Hassan received the Ph.D. degree from the University of New Brunswick, Fredericton, NB, Canada, in 2008.

He is a Professor with the Department of Geomatics Engineering, University of Calgary, Calgary, AB, Canada. He focuses on the application of remote sensing in forecasting and monitoring of natural hazards/disasters, such as forest fire, drought, and flooding; use of remote sensing and geographic information system (GIS) techniques in understanding the dynamics of natural resources, such as forestry, agriculture, and water; and integration of remote sensing, GIS, and modeling techniques in addressing issues related to energy and environment.